Volcanic and Solar Forcing of Climate Change during the Preindustrial Era

Drew T. Shindell[1,2], Gavin A. Schmidt[1,2], Ron L. Miller[1,3], and Michael E. Mann[4]

[1]NASA Goddard Institute for Space Studies, New York, NY 10025, USA.
[2]Center for Climate Systems Research, Columbia University, New York, NY 10025, USA.
[3]Department of Applied Physics and Applied Mathematics, Columbia University, New York, NY 10025, USA.
[4]Department of Environmental Sciences, University of Virginia, Charlottesville, VA 22902, USA.

We examine the climate response to variability in volcanic aerosols and solar irradiance, the primary forcings during the preindustrial era in a stratosphere-resolving general circulation model. The best agreement with historical and proxy data is obtained using both forcings, each of which has a significant effect on global mean temperatures. However, their regional climate impacts in the Northern Hemisphere are quite different. While the short-term continental winter warming response to volcanism is well-known, we show that due to opposing dynamical and radiative effects, the long-term (decadal mean) regional response is not significant compared to unforced variability for either the winter or the annual average. In contrast, the long-term regional response to solar forcing greatly exceeds unforced variability for both time-averages, as the dynamical and radiative effects reinforce one another, and produces climate anomalies similar to those seen during the Little Ice Age. Thus, long-term regional changes during the preindustrial appear to have been dominated by solar forcing.

1. Introduction

While climate models have been able to simulate observed global annual average temperature changes during the past 150 years reasonably well, it is much more difficult to reproduce continental-scale patterns of climate variations (Intergovernmental Panel on Climate Change, 2001). Understanding local changes is even more important than understanding global change, as impacts will be felt on continental or smaller scales (hereafter, we apply 'regional' to mean continental in scale). Given the many factors playing a role in climate change since the industrial revolution, it is extremely difficult to unravel the regional climate response to particular forcings during this period. For the few centuries prior to the industrial era, however, externally driven climate change is thought to have been forced primarily by only two factors: variation in solar output and volcanic eruptions (Crowley, 2000; Free and Robock, 1999; Shindell et al., 2001b). These forcings likely played a large role in the so-called Medieval Warm Period (MWP) and Little Ice Age (LIA) epochs of the last millennium, which saw significant climate changes on at least regional scales. Understanding the magnitude and causes of the forced climate variations, and distinguishing them from unforced, internal variability, is important for historical purposes, and is a crucial test for climate models attempting to predict future climate variations.

Many studies have attempted to attribute preindustrial climate change to external forcings, primarily using relatively simple models. Recently, for example, energy balance models have been used to study the global average response (Crowley, 2000; Free and Robock, 1999; Marcus et al., 1999; Reid, 1997). The studies of Free and Robock (1999) and Crowley (2000), which included both solar and volcanic forcings, suggest that volcanic forcing played the dominant role. Studies using general circulation models (GCMs) of various complexity, which allow the investigation of both the global and regional climate

response to external forcing, have generally been restricted to examinations of historical solar forcing (Cubasch et al., 1997; Drijfhout et al., 1999; Shindell et al., 2001b). Here we present GCM simulations of the decadal-to-centennial scale climate response to volcanic forcing, and compare this to the response to solar forcing and to internal, unforced variations.

2. Experimental Setup

Simulations were performed using a version of the Goddard Institute for Space Studies (GISS) GCM containing a mixed-layer ocean with fixed heat transports and a detailed representation of the stratosphere. The model contains parameterized stratospheric ozone photochemistry (Shindell et al., 1999), which includes ozone-related heterogeneous chemistry. Though the model has relatively coarse horizontal resolution (8° latitude by 10° longitude), it can be run for multiple, long simulations and it reproduces the observed recent multi-decadal stratospheric trends, which seem to be closely linked to regional climate change (Shindell et al., 2001a). The mixed-layer ocean attains thermal equilibrium after a few decades, while the timescales in the real ocean can be much longer, and of course does not allow for ocean circulation changes. These features will influence the results, especially in the North Atlantic and the Southern Ocean where heat is transported into the deep ocean. Future simulations will include a full dynamical ocean.

We examine the generalized climate response to volcanic eruptions and its dependence upon the size, time-of-year, and frequency of the eruptions. We compare this with the long-term response to solar forcing as evidenced by the changes between the late Maunder Minimum, a period of very low solar irradiance during the latter part of the 17th century, and a century later (Shindell et al., 2001b). This relatively large solar irradiance change makes an excellent test case

as it occurred prior to sizeable anthropogenic impacts. Furthermore, estimates of its magnitude and timing are documented by both historical observations and cosmogenic proxies. Our previous simulations demonstrated that the model's regional response to solar forcing largely reproduced the solar component of the surface temperature change derived by correlating reconstructions of irradiance and surface temperatures (Shindell et al., 2001b). We now investigate how well we can account for the *total* regional pattern of surface temperature change evident in climate proxy reconstructions of the LIA, focusing on the Maunder Minimum period.

Since precise historical data on the spatial and temporal distribution of aerosols from volcanic eruptions is unavailable, we base our simulations upon more recent observed stratospheric aerosol optical properties (spatial and temporal distribution, effective radius, and optical thickness) using the GISS data set (Hansen et al., 1996; Sato et al., 1993) (Figure 1). The vertical profile of the aerosols covers 15-35 km in 5 km steps and optical properties are described at several key wavelengths (further information available at http://www.giss.nasa.gov/data/strataer/). We have performed an ensemble of five simulations using the observed time series of 1959-1999 eruptions, and three separate runs repeatedly simulating the June 1991 Mt. Pinatubo eruption. To see the effect of a larger aerosol load and different eruption date relative to the seasonal cycle, we also forced the GCM with two estimates of the April 1815 Mt. Tambora eruption. For Pinatubo, aerosols for 1991 through 1997 are based upon observations from the SAGE II satellite. This period includes the Pinatubo eruption and the subsequent 6 years of declining aerosol amounts, to which we add 2 years assuming an exponential decrease in optical thickness with a one year decay constant, and then 3 years with no aerosol loading to make a 12 year eruption/decay time series. To approximate the Tambora eruption, we use the

same time series, but shifted two months earlier and with the aerosol amounts increased by a factor of two or three relative to Pinatubo (the aerosol amount is far more important than the timing of the eruption), which we refer to hereafter as Tambora 2P and 3P, respectively. These aerosol increases are based upon estimates from ice core information calibrated against optical depth information for modern eruptions, which suggests that the forcing from Tambora was roughly twice that of Pinatubo (Crowley, 2000), along with dust veil indices which suggest a factor of three between the eruptions (Robock, 2000). These estimates should capture the climatically relevant stratospheric aerosol more accurately than a volcanic explosivity index, which indicates the strength of the eruption rather than the aerosol injected into the stratosphere. The three volcanic aerosol series were used to drive model simulations in which the eruption/decay cycle was repeated 10 times (120 year simulations) for each case. This repetition allows us to obtain good statistics on the model's response as well as to examine the long-term response to periodic eruptions. For brevity, we emphasize the Tambora 3P run over the 2P run, as the 2P response is largely a muted version of the 3P response. Results are compared with a multi-century (250 year) control run without forcing. All runs began from stable initial conditions taken from an earlier control simulation.

3. Impact of Volcanic Eruptions

The global annual average surface temperature response to volcanic eruptions is cooling, resulting from increased absorption and reflection of incoming shortwave radiation by stratospheric aerosols. Averaging all years of the simulations together, the mean annual average cooling was -0.35 C for the periodic Pinatubo eruption, -0.77 C for the periodic Tambora 2P eruption, -1.09 C for the periodic Tambora 3P eruption, and -0.44 C for the observed 1959-1999

volcanoes. These follow the average instantaneous radiative forcings, which were -0.47, -0.91, -1.39, and -0.44 W/m^2 respectively, almost linearly, though there is a suggestion of slightly larger climate sensitivity in response to the more frequent 1959-1999 eruptions. (The sensitivity might be reduced with the introduction of a dynamical ocean model that is free to transport heat anomalies beneath the mixed layer.)

a Winter Warming

In contrast to the long-term global cooling, large regions of the NH extratropical continents warm in the Pinatubo simulation during winters following eruptions (Figure 2, top). This phenomenon is well known, having been seen in both observations (Kelly et al., 1996; Robock, 2000; Robock and Mao, 1992) and GCM studies (Graf et al., 1994; Hansen et al., 1996; Kirchner et al., 1999; Rozanov et al., 2002; Stenchikov et al., 2002). This arises because volcanic forcing induces a shift towards the high phase of a hemispheric scale dynamic circulation pattern known as the Arctic Oscillation (AO) or Northern Annular Mode (which is analogous to the North Atlantic Oscillation in the Atlantic sector, where it is most strongly expressed). During the cold season, this results in enhanced westerly advection of relatively warm oceanic air over the continents and of cooler air from continental interiors to their eastern coasts (Figure 2, top). In some regions, meridional winds are modulated along with the increased westerlies, leading to enhanced warming over Siberia and cooling over the Middle East, for example. Surface temperatures respond oppositely to a low phase, with reduced westerly flow, which allows air from the northeast to flow into Europe, leading to cooling there. We define the model's AO pattern as the leading empirical orthogonal function (EOF) of November to April monthly mean sea-level pressure (SLP) in the control run. The model's control run AO accounts for

26% of the variance in the SLP, similar to the 23% seen in observations (Thompson and Wallace, 1998). SLP differences between the volcanic and control simulations (e.g. Figure 2, bottom) were then projected onto the AO to obtain the mean AO change, which we define as the opposite of the average SLP change poleward of 60° N. Thus an increased AO corresponds to a decrease in Arctic SLP, which is accompanied by an increase in mid-latitude SLP and a strengthening of the westerly zonal winds around 50° -70° N. Note that we saw no significant changes in AO variability in our experiments, and throughout this paper a change in the AO refers to a change in the mean state rather than in the variability.

The average response for the ten winters immediately following the Pinatubo eruptions is an AO increase of 1.8 ± 0.9 mb at the 95% confidence level. While the results are statistically significant, the AO response in individual simulations ranged from -2.0 to +4.4 mb. Assuming this range is realistic, comparison with a single real-world realization (an observed AO increase of 0.9 mb following Pinatubo relative to the previous 7 years) is of limited value (the probability of a positive response of any size is 85%, and the two standard deviation range of a single eruption is –1.2 to +4.8). Similarly, the range of responses seen in the second year following the Pinatubo eruption was quite large (–1.5 to +1.8). The difference between the observed 1992/93 increase of 1.8 mb in the AO and the model's mean response of no AO change is thus within expected interannual variability. The observed winter response averaged over several eruptions provides better statistics, though since the aerosols injected by each eruption are different, the comparison is still imperfect. An analysis of pressure observations during the winter following the four largest tropical eruptions of the last 150 years shows a similar pattern to that seen in the GCM, with statistically significant SLP changes of -4 to -6 mb over the Arctic and +2 to

+4 mb over Europe during winter (Kelly et al., 1996). Note that the model's SLP changes are larger in winter (December-February) than in the broader November-April average, with decreases of 3-7 mb over the Arctic, in accord with the observations. Additionally, both the GCM and the observations show a decrease in SLP of -1 to -3 mb over North America (statistically significant in the observations, marginally so in the GCM for December-February), breaking the zonal symmetry of the changes.

We can also compare the surface temperature response with observations. An analyses of measurements following the 12 largest eruptions during the 19th and 20th centuries shows statistically significant responses in several regions, namely a warming of more than 2 C over north-central Siberia, a 0.5-1 C warming over the central United States, and weak (<1 C) cooling in the Middle East (Robock and Mao, 1992). The analysis of Kelley et al. (1996) finds very similar results, also including a statistically significant cooling of -2 to -4 C at the eastern tip of Siberia (Robock and Mao find a similar cooling in this region, though theirs is not statistically significant). The model's surface temperature response compares reasonably well with these values (Figure 2, top). The model underestimates the warming over North America. However, the impact of the AO is less pronounced in this area than over Eurasia, making the signal harder to discern in both observations and the model. Overall, our ability to reproduce the large dynamical perturbation in the winter immediately following eruptions increases our confidence in the GCM's longer-term dynamical response to volcanic forcing.

For the year following the eruption, the 1.4 ± 0.9 mb AO response in the Tambora 3P simulation or the 1.3 ± 0.8 mb AO response in the Tambora 2P simulation are statistically indistinguishable from the Pinatubo response, although the surface temperature responses are quite different (Figure 3). The Tambora

eruption was much larger than Pinatubo (and occurred earlier in the year). The direct radiative forcing dominates the net surface temperature changes in the 3P simulation, leading to significant cooling throughout most of the Northern Hemisphere (NH) despite the positive AO. Dynamical and radiative perturbations are more nearly balanced in the 2P simulation, which produces a response that is fairly similar to the Pinatubo simulations, though superimposed upon a larger radiative cooling. The hemispheric mean temperature for the year following the eruption dropped by 0.7 C in the 3P case, and by 0.5 C in the 2P case, comparable to (especially 2P) observation-based estimates for 1816 (Jones and Bradley, 1992), known as 'the year without a summer' in Europe and eastern North America. Modeled continental cooling following Tambora's eruption is generally slightly larger during summer than during winter, especially over Siberia and the central United States where the AO impacts are largest, due to the rapid land temperature adjustment to the larger summertime solar forcing and the absence of dynamical warming (Figure 4). Similar seasonality is seen in the Tambora 2P case. Note that the dynamically induced winter continental warming tendency partially offsets the enhanced radiative summer cooling over the continents, so that in regions where the dynamical impact is largest such as Siberia or the central US, the annual average response is weaker than over other continental areas. However, there is still a very strong pattern of cooling maximizing over continental areas in the Tambora 3P case, which contrasts greatly with the annual average response to Pinatubo that clearly shows the winter warming pattern (Figure 4). Annual average results from the Tambora 2P simulations fall approximately midway between the other runs, as for the wintertime.

b Physical Mechanisms

The radiative impact of volcanic aerosols is both to cool the surface and to warm the lower stratosphere. After Pinatubo, the model simulates a large winter warming in the sunlit portion of the lower stratosphere (~2 C), similar to NCEP observations (Stenchikov et al., 2002). This increases the meridional temperature gradient between mid-latitudes and the Arctic in that region. Since the eruption takes place in June, the ocean is given relatively little time to adjust to the radiative forcing by the following winter, and the tropical surface cooling then is only -0.1 C. This leads to a very small cooling of the tropical upper troposphere (due to its close connection with the surface in convective regions), which marginally reduces the meridional temperature gradient in the tropopause region due to the reduction of tropopause height with increasing latitude. However, this has a weaker impact than the much larger lower stratospheric heating in the sunlit atmosphere at slightly higher altitudes. The gradient change increases the westerly winds in this region, which refracts upward propagating planetary waves towards the equator (Shindell et al., 2001a). This in turn leads to an increase in poleward angular momentum flow, which drives the stronger surface westerlies associated with a positive AO anomaly. This dynamical planetary wave feedback via the stratosphere has been seen in response to volcanic eruptions in both observations and GCM simulations (Kodera, 1994; Perlwitz and Graf, 1995; Shindell et al., 2001a). The warming associated with the enhanced AO is large enough to offset most of the surface cooling in the extratropics for the Pinatubo simulation, so that the net change in the year after the eruption (July 1991-June 1992) is -0.1 C averaged over the entire NH extratropics (Figure 4). This is similar to observations and other GCM simulations (Hansen et al., 1996; Kirchner et al., 1999; Robock and Liu, 1994; Robock and Mao, 1995).

The modeled ozone changes in response to Pinatubo aerosol are broadly similar to those observed (Randel et al., 1995), with around 10% column

depletion polewards of 60° N during the boreal late winter to spring and about 4% loss at NH mid-latitudes. These losses result primarily from heterogeneous chemical activation of chlorine due to the increased surface area provided by volcanic aerosols, as in other models (Al-Saadi et al., 2001; Rozanov et al., 2002). To examine the influence of the ozone changes on the dynamics, a second Pinatubo run was performed without ozone changes (sixty year length). This showed a similar AO response averaged over the entire winter, though the ozone depletion in the original Pinatubo simulation reduced the AO response in the early winter months (cooling of the sunlit lower stratosphere offsetting a portion of the aerosol heating) and enhanced the response in the late winter (larger ozone loss in the polar regions causing cooling there). An enhancement of the AO during the late winter and early spring due to volcanic-induced Arctic ozone depletion has also been reported in other simulations (Stenchikov et al., 2002).

In the Tambora experiments, the atmospheric composition was changed to preindustrial conditions for the chemistry calculations. In such an atmosphere, with no anthropogenic chlorine, aerosol effects are minimal. The main effect of heterogeneous processing is then to remove nitrogen oxides from the lower stratosphere. This allows more hydrogen oxide radicals to exist, however. Because these influence ozone in opposite directions, the net impact is quite small (the Tambora runs showed ozone changes less than one-fifth the Pinatubo changes). We therefore did not include ozone changes in the transient 1959-1999 ensemble, as these were designed to be used as representative simulations of the potential preindustrial climate response to volcanism.

As noted, the AO response to Tambora is similar to the response to Pinatubo for the first winter, but the surface cooling is much larger. The increased meridional temperature gradient due to the aerosol heating in the lower stratosphere is partially offset by the cooling of the tropical upper troposphere,

which reduces the meridional temperature gradient in the tropopause region. Thus despite the much larger forcing, the AO response is approximately the same magnitude as for Pinatubo. The net change in NH extratropical surface temperatures for the year after the Tambora eruption (using July-June, as for Pinatubo) is -0.8 C in the 3P simulation (Figure 4), demonstrating that unlike after Pinatubo, the radiative cooling dominates over the dynamical AO related warming. The radiative forcing remains strong for several years due to the large size of the eruption. By the third year in the 3P simulation, the aerosol heating of the lower stratosphere has declined from the 3-4 C seen in the first winter to a cooling of -0.04 C, while the upper tropical troposphere has cooled substantially (-2 C) as the ocean adjusts more fully to the aerosol forcing. This leads to a reduced latitudinal temperature gradient in the tropopause region, resulting in a reduction of the westerly winds and a decrease in the AO (Figure 5). While this appears over most of the years after the second, it only approaches statistical significance in the third year, at the time when the ocean response is largest. The Tambora 2P simulation also shows a marginally statistically significant response in its second year (Figure 5). Given that there are 33 data points, random chance would give 1.7 significant points at the 95% confidence limit, so we believe that for individual years only the positive AO seen consistently in all three simulations is robust. Averaging over years 3 to 11, however, all three simulations show a statistically significant negative AO response.

The long term dynamical response is thus a combination of the initial positive AO forced by stratospheric heating and the delayed negative AO response forced by tropical surface cooling. Projecting the average SLP change between the volcanic runs and the control onto the control EOFs gives a twelve year average AO response of -0.2 ± 0.4 mb for the Pinatubo simulation, and -0.8 ± 0.5 mb and -0.5 ± 0.4 mb for the Tambora 3P and 2P simulations, respectively. For the more

frequent volcanic eruptions during the 1959-1999 period, the ensemble average response is 0.3 ± 0.1 mb. Thus the long-term response appears to be quite small compared to unforced decadal scale variability, except perhaps in the case of extremely large eruptions such as Tambora 3P.

4. Comparison of Volcanic and Solar Forcings

In contrast to volcanic eruptions, long-term decreases in solar irradiance lead to a strong negative AO response in our model (Shindell et al., 2001b); a 1.1 ± 0.4 mb decrease for the Maunder Minimum versus a century later which causes significant wintertime continental cooling (Figure 6). A similar signal is present in the summer (Figure 6) due to the long-term persistence of SST anomalies and radiative cooling of the continents, but with reduced amplitude compared with the winter since there is no dynamical enhancement. Another GCM has also reported an enhanced temperature response to solar forcing over NH continents, consistent with a reduced AO (Cubasch et al., 1997). The two primary forcings for climate in the preindustrial period, solar variations and volcanic eruptions, thus have quite different impacts in the model. For both volcanic eruptions and decreased solar irradiance the global average response is cooling. The regional responses are dissimilar, however (Figure 6). The long-term effect of volcanic eruptions on regional surface temperature changes is extremely small, owing to the cancellation of dynamical and radiative patterns of spatial response. Comparison of two historical periods would likely yield even less response to volcanic eruptions than in the simulations discussed above, which are with respect to a control run with zero volcanic activity. For regional changes, a significant negative AO anomaly on decadal timescales is forced by volcanoes only in the event of very large eruptions, for which tropical surface and tropospheric cooling overwhelm the heating by stratospheric aerosols. Such eruptions occur extremely rarely, however,

Tambora being the largest eruption in 500 years. Note that while large high-latitude eruptions may also affect the AO and surface climate for a year or two (Graf and Timmreck, 2001; Robock and Mao, 1995), they would be expected to show a similar lack of spatial inhomogeneity in their long-term responses.

Solar and volcanic forcings induce such different responses because the stratospheric and surface influences in the solar case reinforce one another but in the volcanic case are opposed. Decreased solar irradiance cools the surface. At the same time, the lower stratosphere cools due to decreased absorption of incoming solar radiation by ozone owing to both the irradiance reduction and to reduced photochemical production of ozone in the lower stratosphere. In the example of the Maunder Minimum versus a century later, the sunlit portion of the lower stratosphere cooled by 0.2 to 0.4 C during winter. The upper tropical troposphere cooled by 0.6 to 0.8 C in response to the tropical surface cooling. These persistent coolings led to a reduced temperature gradient between NH middle and high latitudes in both the lower stratosphere and the upper troposphere, forcing a negative AO (Shindell et al., 2001b). In contrast, volcanic eruptions cool the surface, but aerosol heating warms the sunlit lower stratosphere. This leads to an increased meridional gradient in the lower stratosphere, but a reduced gradient in the tropopause region. These may separately cause enhancements of the AO on one to two year timescales via the stratospheric warming, and reductions on decadal timescales via the surface cooling. However, in light of these opposing physical drivers of AO changes, and the short-term nature of the large dynamical response to eruptions (Figure 5), it is not surprising that the long-term net dynamical effect of volcanic eruptions is minimal. Additionally, the typically short timescale of volcanic perturbations does not allow their radiative impact to be fully felt by the oceans or sea ice, in contrast to multi-decadal solar forcing, further weakening their long-term effect. Since the impact of the volcanically-

16

induced dynamical changes on the annual average temperatures is also reduced by the seasonally opposed influences of the radiative response (summer continental cooling) and stratospherically-forced dynamical response (winter continental warming), it is reasonable that the long-term annual average impact of volcanoes is relatively homogeneous spatially.

5. External Forcing of Historical Climate Change

a Regional Changes

Since the global average surface temperature response basically follows the radiative forcing for both volcanic and solar forcing (the model is slightly more sensitive to solar than to volcanic forcing due to positive feedbacks from stratospheric ozone and the AO response), relatively simple models such as energy balance models can give reasonable estimates of global mean temperature variations in past centuries. Given that the regional response is not always a simple function of the radiative forcing, more complex models such as GCMs are required to investigate regional climate change. All climate models are limited by the accuracy to which the historical forcing is known. While paleoindicators give an idea of the size of past eruptions, the spatial distribution of the aerosols and the exact timing of some eruptions are not well known. However, examining our ensemble of simulations driven by observed 1959-1999 eruptions, we find a good correlation between the global surface temperature response and the total forcing for decadal time scales. Though our sample is small (4 decades), this suggests that the global response may not be greatly sensitive to the precise details of the aerosol distribution. More importantly, spatial inhomogeneities are relatively small. Comparison of the ensemble mean pattern of surface temperature anomalies relative to the zonal mean for each decade against the same pattern for the

remaining decades shows no more areas of statistically significant correlations (95% level) than random noise outside of a warming over Europe and a cooling in the Bering Strait region. This argues against the presence of major regional anomalies associated with volcanically forced changes in the zonal flow in other areas.

b The Maunder Minimum

The simulated external forcing of regional surface temperature anomalies can also be compared with patterns derived from a compilation of diverse proxy climate indicators. We use model results from simulations forced with reduced solar irradiance during the Maunder Minimum compared with a century later, and from our volcanic simulations (the 20th century transients, Pinatubo, and Tambora-3P). The latter serve as a generalized response to volcanic forcing, which was ~0.16 W/m^2 more negative during the late 17th century (1660-1690) than the late 18th century (1770-1790) (Crowley, 2000). Proxy data have been averaged over these same decades to obtain decadal timescale patterns.

We compare the response in regions that exhibit large, coherent variations in the proxy-data record (Figure 7). The unforced variability is the 1-sided 95% confidence range for the occurrence of a regional anomaly of the same sign as the proxy data in any single 25-year period in the 250-year control run. The decadal-scale regional response in all the volcanic experiments is extremely weak. The only significant responses are over Europe for the transient, over Europe and the North Atlantic for Pinatubo, and over Europe and North America for Tambora 3P. Aside from the European warming, it is clear that there is no consistent pattern of regional surface response to volcanic forcing in these areas. Additionally, there is no evidence of a response which scales with the forcing, which ranges from -0.25 W/m^2 during 1969-1978 to -1.39 W/m^2 for Tambora 3P.

Using the mean response over the four decades of the transient ensemble as broadly representative of the influence of volcanic activity, the volcanic response is well within the range of the unforced variability in all regions except Europe. This occurs despite a relatively large average forcing of -0.44 W/m^2. In contrast, the solar forcing causes a large, statistically significant response in each region which has the same sign as the proxy-data and exceeds unforced variability. Though these simulations may underestimate unforced variability on long timescales due to the lack of a dynamic ocean, our results are consistent with results from a comparison between climate proxies and an unforced run of the Hadley Center coupled GCM (Collins et al., 2002) which also suggests that the majority of preindustrial climate change over NH mid-to-high latitude continents results from solar and volcanic forcing.

While paleoclimate reconstructions of surface temperatures in past centuries are uncertain, there is broad agreement among different methods and data sources, at least at the level of the NH mean temperature variations (Briffa et al., 1998; Crowley, 2000; Jones et al., 1998; Mann et al., 1999). On the regional scale, European temperature estimates are most reliable, as historical and a few long instrumental data series augment the more widespread proxy-data such as tree-rings in the proxy network reconstruction. The reconstructed European regional temperature anomaly is thus a key test of a model's regional response to forcing. Comparing the Maunder Minimum period with a century later, the more negative volcanic forcing fails to produce even the right sign of temperature change in this region, as all the volcanic simulations generate a warming relative to the NH extratropical mean while the proxy data and the response to solar forcing show cooling outside the range of unforced variability (Figure 7).

The reconstructed volcanic forcing during the late Maunder Minimum as compared with the late 18th century is only about one-quarter the mean 1959-

1999 volcanic forcing of -0.66 W/m^2 in the same reconstruction (Crowley, 2000). Since the Sato et al data do not extend back before 1850, we use the Crowley reconstruction in our discussion of the centennial scale influence of volcanic forcing on climate. We believe, however, that it may represent a high-end estimate of the volcanic forcing during the past millennium (Sato et al., 1993; Crowley, 2000).

Assuming that the responses can be linearly summed (given that the long-term volcanic influence on the non-linear AO/NAO and hence on regional changes is very weak), the surface temperature response to a forcing of this magnitude, estimated simply as one-quarter the response during the 1959-1999 experiments, can be added to that due to reconstructed solar irradiance changes during this same period (Lean et al., 1995). This provides an estimate of the total change (Figure 8). The result shows a regional pattern of continental cooling due to a forced negative AO anomaly. While the global mean change is 75% due to solar forcing and 25% to volcanic forcing, all of the AO reduction is attributable to the solar forcing, as the volcanic forcing actually gave a weak AO increase.

We compare the total response with that derived from surface temperature pattern reconstructions based on diverse proxy data (Mann et al., 1998). A favorable agreement is found between the simulated and reconstructed temperature anomalies over this period (Figure 8), with both showing large, spatially coherent anomalies in mid-latitudes. Agreement is especially good over North America, where the impact of reduced northwesterlies moving around the Rockies is clearly visible in both cooling patterns. The model also reproduces the cooling which arcs up through western Europe into Asia, though the Middle East does not show the warming seen in the reconstruction (it is relatively warm compared to Eurasia, however). While both the GCM and the reconstruction show warming over parts of the North Atlantic, the reconstructed anomaly is less than the unforced

variability, which is quite large in this region. Additionally, we regard the model simulation results as being less reliable over the oceans, as they do not include changes in ocean dynamics, which may be an important feedback, at least in the Atlantic where surface anomalies are buffered by communication with the deep ocean (Delworth and Dixon, 2000). The model results also don't account for possible changes in the El Nino/Southern Oscillation and potential extratropical responses, particularly with regard to the Pacific region. Nevertheless, the basic pattern of anomalously cold continents is clear in both the paleoclimate data and the model response, and it is in these areas that both values are most reliable. The amplitude of the cooling is larger in the model, however. This version of the GISS GCM has a climate sensitivity at the high end of the modeled range (~1 per W/m^2). Additionally, the proxy reconstruction is implicitly spatially smoothed through the use of a limited eigenvector basis set to approximate large-scale temperature changes. Moreover, data availability limits the size of this basis set in earlier centuries, leading to a greater smoothing of regional temperature variations prior to the 18th century in particular. Note that there is some independent evidence for a reduced NAO during the late 17th and 18th centuries from European historical reconstructions (Luterbacher et al., 1999). Additional support for Atlantic sector circulation change consistent with a reduced AO/NAO during the LIA comes from sediment cores (Kiegwin and Pickart, 1999) and from historical evidence for greater northeasterly flow of continental air into Europe (Wanner et al., 1995). Other proxies which have been related to North Atlantic climate variability also appear to be correlated with solar variations on millennial time scales (Bond et al., 2001). Based on our simulations, we caution that very large eruptions may add difficulty to reconstructing past AO or NAO indices based on temperature proxies since the rapid continental response to very large

radiative forcing yields a pattern of relatively cold continents during winter despite the positive AO/NAO in the Tambora 3P run (Figure 3).

c Centennial Scale Climate Change

The relative importance of volcanic and solar forcing to long-term climate change can be examined more broadly by comparing the reconstructed forcings (Crowley, 2000) across other time periods. The 17th century average is representative of the LIA. Compared with the period 1850-1899, before the bulk of the anthropogenic forcing, the 17th century solar forcing anomaly is estimated to be -0.19 W/m^2 while the volcanic is -0.30 W/m^2. Compared with the period 1000-1299, which coincides with warmer hemispheric mean temperatures (Briffa et al., 1998; Jones et al., 1998; Mann et al., 1999) and the MWP, both the 17th century solar and volcanic forcings were -0.16 W/m^2. In both cases, the volcanic forcing was at least as large as the solar. Since the global temperature change follows the radiative forcing fairly closely, this suggests that the volcanic impact on the global mean LIA cooling was important, as previously hypothesized (Crowley, 2000; Free and Robock, 1999). The global mean response to the combined solar and volcanic forcing exceeds the unforced variability, which is ~0.19 C (95% confidence interval), by a factor of 2 to 2.5 for the LIA and MWP. Although the climate sensitivity of this version of the GCM is relatively high, the forced component would still exceed the unforced with a more typical sensitivity of ~3/4 C per W/m^2, suggesting that much of the variability seen in climate reconstructions does not arise merely from internal chaotic variations. We reiterate, however, that the absence of a fully coupled ocean in these experiments may limit the internal variability.

The presence of a sizeable decrease in solar irradiance during the LIA relative to the MWP or the latter half of the 19th century implies a significant regional cooling over mid-latitude NH continental areas. On the regional scale, the solar-induced anomalies scaled to the LIA forcing (roughly one-half the -0.32 W/m^2 difference in the late Maunder Minimum versus a century later simulations) would be of the appropriate sign and in excess of the unforced variability in both Europe and North America (Figure 7). The appropriately scaled volcanic-induced anomalies (about 1/3 to 2/3 the forcing in the 1959-1999 transients) would not meet these criteria in any region. The modeling results show continental changes 1.5 to 3 times the NH mean change in response to a total forcing which is roughly two parts solar to one part volcanic (Figure 8). While the solar-to-volcanic ratio is between two-thirds and one for the forcing change between the LIA and the MWP or between the LIA and the latter half of the 19th century, this still leads to continental cooling roughly 1.3 to 2.5 times larger than the NH mean.

Such differences between the NH mean and the continental interiors are in accord with the contrast between reconstructions of full NH (land and ocean, tropics and extratropics) annual mean temperature changes in past centuries based on diverse proxy ('multiproxy') data (Crowley and Lowery, 2000; Jones et al., 1998; Mann et al., 1998; 1999) and extratropical NH temperature reconstructions based on tree-ring data alone (Briffa et al., 1998; Esper et al., 2002). These latter reconstructions are representative of the more restricted continental regions of the NH, and target warm-season temperatures through the tree-ring species and parameters employed in the reconstructions (Mann and Hughes, 2002). Due to the seasonally and spatially varying surface temperature responses to solar and volcanic forcing discussed earlier, continental proxies sensitive to warm-season temperatures emphasize the enhanced continental summer cooling associated with the radiative response to volcanic forcing, but miss the often-present dynamical

continental winter warming in response to those same events. This seasonal sensitivity thus effectively rectifies the temperature response to volcanic forcing, exaggerating the recorded hemispheric (land and ocean) cooling associated with volcanic forcing (Mann, 2002). For these reasons, tree-ring based continental temperature reconstructions show evidence of far greater cooling in response to individual volcanic events (Briffa et al., 1998) and greater cooling on multidecadal-to-century timescales (Esper et al., 2002) than full hemispheric reconstructions. Our results suggest that these differences do not require any additional extratropical forcing or internal multi-century oscillations (Bradley et al., 2001; Broecker, 2001; Esper et al., 2002), as they can be accounted for by the dynamical response to both volcanic and solar variations.

6. Conclusions

Volcanic forcing is important for both regional climate change on a year-to-year basis, and for long-term climate change on a global scale. It appears unlikely to induce sustained regional climate changes that exceed unforced variability, however. In contrast, solar forcing creates long-term regional climate changes that are greater than unforced variability, and which resemble those seen in proxy-based reconstructions of historical temperature change during the Maunder Minimum. The regional anomalies result primarily from a forced shift in the AO.

During the last several decades, there has been an apparent upward trend in the AO (Thompson and Wallace, 1998). Solar forcing, however, has increased little if at all over this period, by less than 0.05 W/m^2 since the 1960s (the exact value depends upon the particular years chosen for the trend calculations). Such a small increase in irradiance would cause an AO enhancement of about 0.1 mb, much smaller than the apparent trend of 3 mb, which is more likely to be

attributable to increases in greenhouse gases, and to a lesser extent, Arctic ozone depletion (Shindell et al., 2001a).

Downward shifts in the AO are closely correlated with cold temperature extremes in Europe (Higgins et al., 2002; Thompson and Wallace, 2001), consistent with the historical impression that the LIA in Europe was punctuated by short periods of extreme cold exceeding than that seen in the multi-decadal averages of proxy-data shown here (Pfister, 1995). The global mean "Little Ice Age" signal can therefore be attributed to both volcanic and solar forcing, but while volcanic forcing may have played a major role in global-scale cooling, the much larger regional changes and probable changes in the frequency of extreme cold events were likely driven primarily by solar variability.

Figure 1. Time series of zonal mean stratospheric aerosol optical thickness at 550nm used in the transient volcanic experiment. The latter portion of these data are derived from SAGE II satellite observations. The last 9 years, followed by three years with no aerosol loading, were used to create the 12 year series used to repeatedly force the GCM for the Pinatubo and Tambora experiments.

Figure 2. Average winter surface temperature response (December-February, top) and sea-level pressure (November-April, bottom) in the ten winters immediately following eruptions for Pinatubo. Temperature responses are significant in the subtropics for values greater than about 0.3 K, and at mid-latitudes for values greater than about 1.0 K, while the response poleward of ~75 N is not significant. See text for the statistical significance of the AO (SLP) response.

Figure 3. As in figure 2, but for the Tambora simulations. Temperature changes in excess of about 0.4 K in the subtropics and about 0.9 K at mid-latitudes are statistically significant for both runs. See text for the statistical significance of the AO (SLP) response. The sea-level pressure response pattern in the Tambora 2P simulation is extremely similar to the 3P result.

Figure 4. Surface temperature response during the years immediately following eruptions. Values are given for the summer (June-August) average for Pinatubo (top left) and Tambora 3P (bottom left) and for the annual average for Pinatubo (top right) and Tambora 3P (bottom right).

Figure 5. The mean AO response as a function of year after the Pinatubo and Tambora eruptions. Values are pressure averaged northward of 60° N relative to the mean for each simulation, which is 0.6 (0.2) mbar lower in the Tambora 3P

(2P) simulation due to overall negative forcing of the AO. Solid horizontal lines show the 95% confidence level for the mean AO response for ten realizations.

Figure 6. Surface temperature response (K) to decreased solar irradiance during 1680 relative to 1780 and in the volcanic transient experiments. Values are given for the solar simulations for November-April (top left), May-October (bottom left), and the annual average (top right). The annual average over the 5 ensemble members of the transient volcanic runs (1959-1999) is shown for comparison (bottom right). Note the difference in scale between the two columns. Cold-season temperature responses are significant in the subtropics for values greater than about 0.2 K, at mid-latitudes for values greater than about 0.3 K, and poleward of ~75 N for values greater than about 0.6 K. Warm-season and annual average values greater than about 0.2 to 0.3 K are significant. The solar forcing was –0.32 W/m^2, while the average volcanic forcing was –0.44 W/m^2.

Figure 7. Long-term regional annual average surface temperature changes. The upper bars show the mean regional response to volcanic forcing in the transient ensemble for the 1960s (1959-1968), 1970s (1969-1978), 1980s (1979-1988), and from the Pinatubo and Tambora 3P simulations. Decades were chosen so as to exclude large volcanic eruptions in the last two years, which would impact the radiative forcing but not yet be fully felt by the climate system. Values for all temperature changes are given for the outlined regions as shown on the lower map compared to the mean change in the Northern Hemisphere extratropics.

The lower section shows 1660-1690 versus 1770-1790 regional temperatures in the multiproxy resonstruction. Model results for solar forcing changes are shown for the same time period. The volcanic response is averaged over the 1960s to 1990s (forcing = -0.44 W/m^2) as indicative of the long-term

response to sizeable volcanic activity. The 95% confidence levels for the decadal volcanic transients are .15 C for North America, .18 C for the North Atlantic, .07 C for Europe, and .12 C for Siberia. They are ~.05 C for the longer Pinatubo, Tambora, and solar simulations. Note that the statistical significance of the GCM results comes from a signal-to-noise comparison over a large number of experiments. Thus the response can be significant while still being less than the unforced variability range of any one 2-3 decade period (see text for unforced methodology).

Figure 8. Reconstructed (top) and simulated (bottom) annual average temperature difference between 1660-1680 and 1770-1790. The reconstructed surface temperatures are based on a multi-proxy estimate using tree-rings, ice cores, corals and historical data (Mann et al., 1998). Model results are based on the sum of the response in two simulations, one incorporating reconstructed solar irradiance changes during this period and one using volcanic forcing scaled to changes over this time.

Al-Saadi, J., R. B. Pierce, T. D. Fairlie, M. M. Kleb, R. S. Eckman, W. L. Grose, M. Natarajan, and J. R. Olson, 2001: Response of middle atmosphere chemistry and dynamics to volcanically elevated sulfate aerosol: Three-dimensional coupled model simulations. *J. Geophys. Res.*, **106,** 27255-27275.

Bond, G., et al., 2001: Persistent solar influence on North Atlantic climate during the Holocene. *Science*, **294,** 2130-2136.

Bradley, R. S., K. R. Briffa, T. J. Crowley, M. K. Hughes, P. D. Jones, and M. E. Mann, 2001: Scope of Medieval Warming. *Science*, **292,** 2011-2012.

Briffa, K. R., P. D. Jones, F. H. Schweingruber, and T. J. Osborn, 1998: Influence of volcanic eruptions on Northern Hemisphere summer temperature over the past 600 years. *Nature*, **393,** 350-354.

Broecker, W. S., 2001: Was the Medieval Warm Period Global? *Science*, **291,** 1497-1499.

Collins, M., T. J. Osborn, S. F. B. Tett, K. R. Briffa, and F. H. Schweingruber, 2002: A comparison of the variability of a climate model with paleotemperature estimates from a network of tree-ring densities. *J. Climate*, **15,** 1497-1515.

Crowley, T. J., 2000: Causes of climate change over the past 1000 years. *Science*, **289,** 270-277.

Crowley, T. J. and T. S. Lowery, 2000: How warm was the medieval warm period? *Ambio*, **29,** 51-54.

Cubasch, U., R. Voss, G. C. Hegerl, J. Waszkewitz, and T. J. Crowley, 1997: Simulation of the influence of solar radiation variations on the global climate with an ocean-atmosphere general circulation model. *Clim. Dynam.*, **13,** 757-767.

Delworth, T. L. and K. W. Dixon, 2000: Implications of the recent trend in the Arctic/North Atlantic oscillation for the North Atlantic thermohaline circulation. *J. Climate*, **13,** 3721-3727.

Drijfhout, S. S., R. J. Haarsma, J. D. Opsteegh, and F. M. Selten, 1999: Solar-induced versus internal variability in a coupled climate model. *Geophys. Res. Lett.*, **26,** 205-208.

Esper, J., E. R. Cook, and F. H. Schweingruber, 2002: Low-frequency signals in long tree-ring chronologies for reconstructing past temperature variability. *Science*, **295,** 2250-2253.

Free, M. and A. Robock, 1999: Global warming in the context of the Little Ice Age. *J. Geophys. Res.*, **104,** 19057-19070.

Graf, H.-F., J. Perlwitz, and I. Kirchner, 1994: Northern Hemisphere tropospheric mid-latitude circulation after violent volcanic eruptions. *Beitr. Phys. Atmos.*, **67,** 3-13.

Graf, H. F. and C. Timmreck, 2001: A general climate model simulation of the aerosol radiative effects of the Laacher See eruption (10,900 BC). *J. Geophys. Res.*, **106,** 14747-14756.

Hansen, J. E., et al., 1996: A Pinatubo climate modeling investigation, in The Mount Pinatubo Eruption: Effects on the Atmosphere and Climate. *NATO ASI Series Vol. I*, G. Fiocco, D. Fua, and G. Visconti, Eds., Springer-Verlag, 233-272.

Higgins, R. W., A. Leetmaa, and V. E. Kousky, 2002: Relationships between climate variability and winter temperature extremes in the United States. *J. Climate*, **15,** 1555-1572.

Intergovernmental_Panel_on_Climate_Change, 2001: *Climate Change 2001*. Cambridge University Press, 881 pp.

Jones, P., et al., 1998: High-resolution palaeoclimatic records for the last millennium: interpretation, integration and comparison with General Circulation Model control-run temperatures. *Holocene*, **8,** 455-471.

Jones, P. D. and R. S. Bradley, 1992: Climatic variations in the longest instrumental records. *Climate Since A.D.1500*, P. D. Jones and R. S. Bradley, Eds., Routledge, 246-268.

Kelly, P. M., P. D. Jones, and J. Pengqun, 1996: The spatial response of the climate system to explosive volcanic eruptions. *Int. J. Clim.*, **16,** 537-550.

Kiegwin, L. D. and R. S. Pickart, 1999: Slope water current over the Laurentian Fan on Interannual to Millennial Time Scales. *Science*, **286,** 520-523.

Kirchner, I., G. L. Stechnikov, H.-F. Graf, A. Robock, and J. C. Antuna, 1999: Climate model simulation of winter warming and summer cooling following the 1991 Mount Pinatubo volcanic eruption. *J. Geophys. Res.*, **104,** 19039-19055.

Kodera, K., 1994: Influence of volcanic eruptions on the troposphere through stratospheric dynamical processes in the Northern Hemisphere winter. *J. Geophys. Res.*, **99,** 1273-1282.

Lean, J., J. Beer, and R. Bradley, 1995: Reconstruction of solar irradiance since 1610: Implications for climate change. *Geophys. Res. Lett.*, **22,** 3195-3198.

Luterbacher, J., C. Schmutz, D. Gyalistras, E. Xoplaki, and H. Wanner, 1999: Reconstruction of monthly NAO and EU indices back to AD 1675. *Geophys. Res. Lett.*, **26,** 2745-2748.

Mann, M. E., 2002: The Value of Multiple Proxies. *Science*, **297,** 1481-1482.

Mann, M. E. and M. K. Hughes, 2002: Tree-Ring Chronologies and Climate Variability. *Science*, **296,** 848-848.

Mann, M. E., R. S. Bradley, and M. K. Hughes, 1998: Global-scale temperature patterns and climate forcing over the past six centuries. *Nature*, **392,** 779-787.

——, 1999: Northern hemisphere temperatures during the past millennium: Inferences, uncertainties, and limitations. *Geophys. Res. Lett.*, **26,** 759-762.

Marcus, S. L., M. Ghil, and K. Ide, 1999: Models of solar irradiance variability and the instrumental temperature record. *Geophys. Res. Lett.*, **26,** 1449-1452.

Perlwitz, J. and H.-F. Graf, 1995: The statistical connection between tropospheric and stratospheric circulation of the Northern Hemisphere in winter. *J. Climate*, **8,** 2281-2295.

Pfister, C., 1995: Monthly temperature and precipitation in central Europe 1525-1979: quantifying documentary evidence on weather and its effects. *Climate Since A.D. 1500. (Revised edition)*, R. S. Bradley and P. D. Jones, Eds., Routledge, 118-142.

Randel, W. J., F. Wu, J. M. Russell, III, J. W. Waters, and L. Froidevaux, 1995: Ozone and temperature changes in the stratosphere following the eruption of Mt. Pinatubo. *J. Geophys. Res.*, **100,** 16753-16764.

Reid, G. C., 1997: Solar forcing of global climate change since the mid-17th century. *Climatic Change*, **37,** 391-405.

Robock, A., 2000: Volcanic eruptions and climate. *Rev. Geophys.*, **38,** 191-219.

Robock, A. and J. Mao, 1992: Winter warming from large volcanic eruptions. *Geophys. Res. Lett.*, **12,** 2405-2408.

Robock, A. and Y. Liu, 1994: The volcanic signal in Goddard Institute for Space Studies three-dimensional model simulations. *J. Climate*, **7,** 44-55.

Robock, A. and J. Mao, 1995: The volcanic signal in surface temperature observations. *J. Climate*, **8,** 1086-1103.

Rozanov, E. V., M. E. Schlesinger, N. G. Andronova, F. Yang, S. L. Malyshev, V. A. Zubov, T. A. Egorova, and B. Li, 2002: Climate/chemistry effects of the Pinatubo volcanic eruption simulated by the UIUC stratosphere/troposphere GCM with interactive photochemistry. *J. Geophys. Res.*, **107,** 4594, doi: 10.1029/2001JD000974.

Sato, M., J. E. Hansen, M. P. McCormick, and J. B. Pollack, 1993: Stratospheric aerosol optical depth, 1850-1990. *J. Geophys. Res.*, **98,** 22987-22994.

Shindell, D., D. Rind, N. K. Balachandran, J. Lean, and P. Lonergan, 1999: Solar Cycle Variability, Ozone, and Climate. *Science*, **284,** 305-308.

Shindell, D. T., G. A. Schmidt, R. L. Miller, and D. Rind, 2001a: Northern Hemisphere winter climate response to greenhouse gas, volcanic, ozone and solar forcing. *J. Geophys. Res.*, **106,** 7193-7210.

Shindell, D. T., G. A. Schmidt, M. E. Mann, D. Rind, and A. Waple, 2001b: Solar forcing of regional climate change during the Maunder Minimum. *Science*, **294,** 2149-2152.

Stenchikov, G., A. Robock, V. Ramaswamy, M. D. Schwarzkopf, K. Hamilton, and S. Ramachandran, 2002: Arctic Oscillation response to the 1991 Mount Pinatubo eruption: Effects of volcanic aerosols and ozone depletion. *J. Geophys. Res.*, **107,** 4803, doi:10.1029/2002JD002090.

Thompson, D. W. J. and J. M. Wallace, 1998: The Arctic Oscillation signature in the wintertime geopotential height and temperature fields. *Geophys. Res. Lett.*, **25,** 1297-1300.

——, 2001: Regional climate impacts of the Northern Hemisphere annular mode. *Science*, **293,** 85-89.

Wanner, H., et al., 1995: Wintertime European circulation patterns during the late Maunder minimum cooling period (1675-1704). *Theor. Appl. Climatol.*, **51,** 167-175.
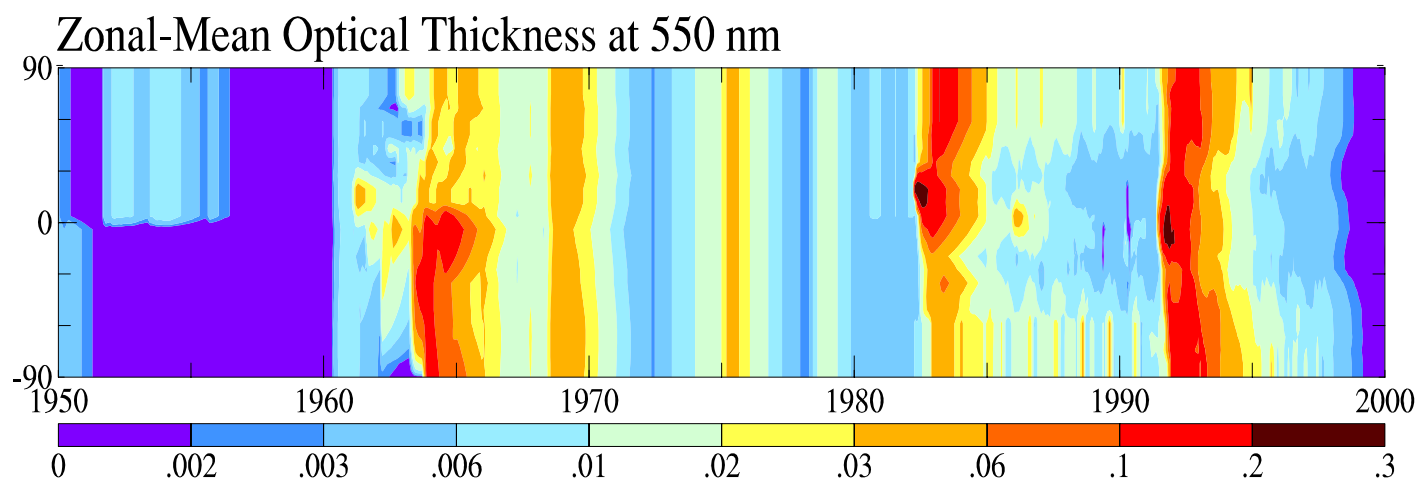
Figure 1

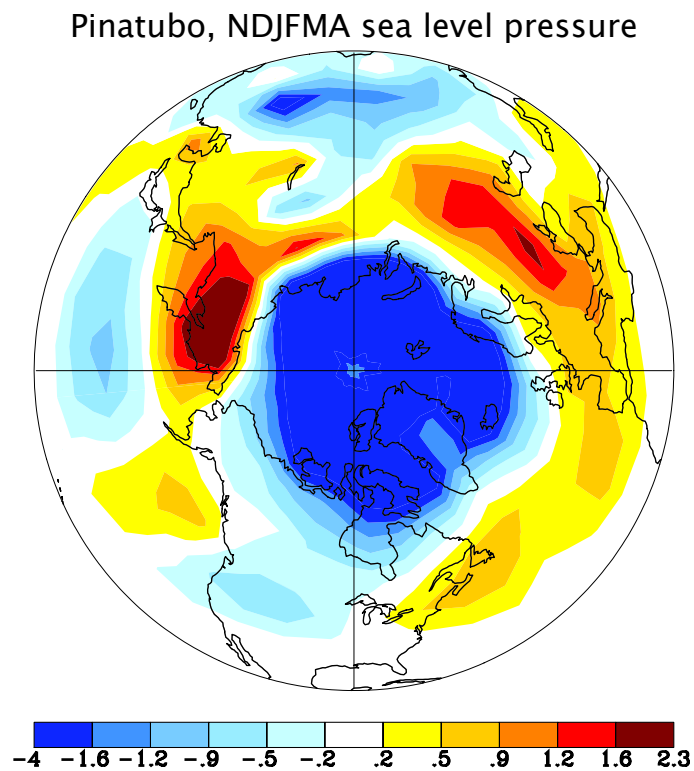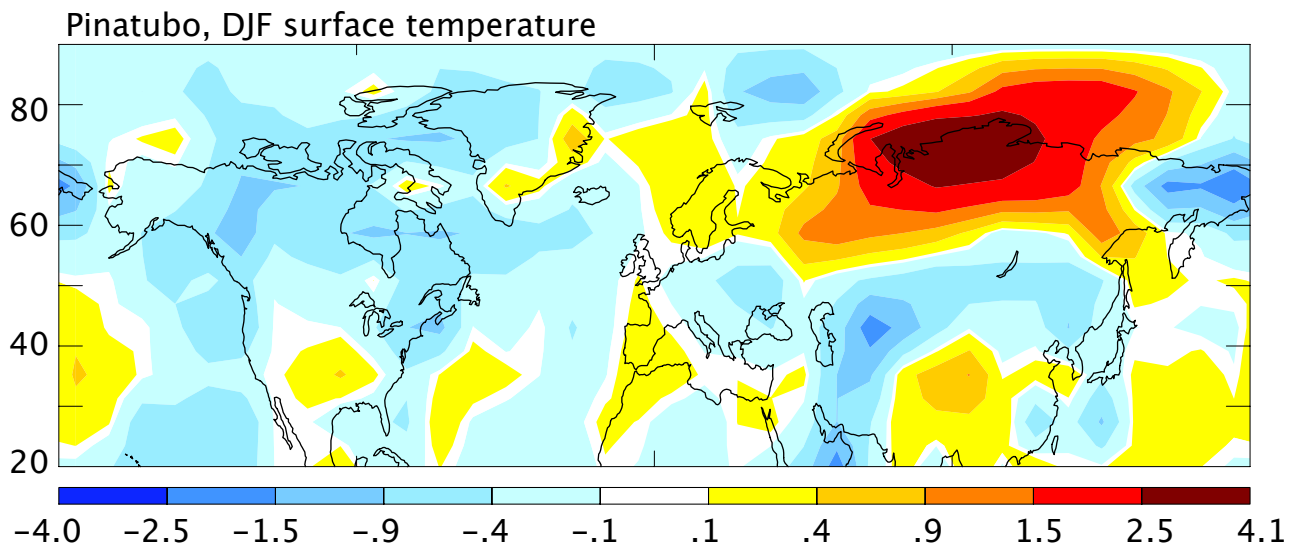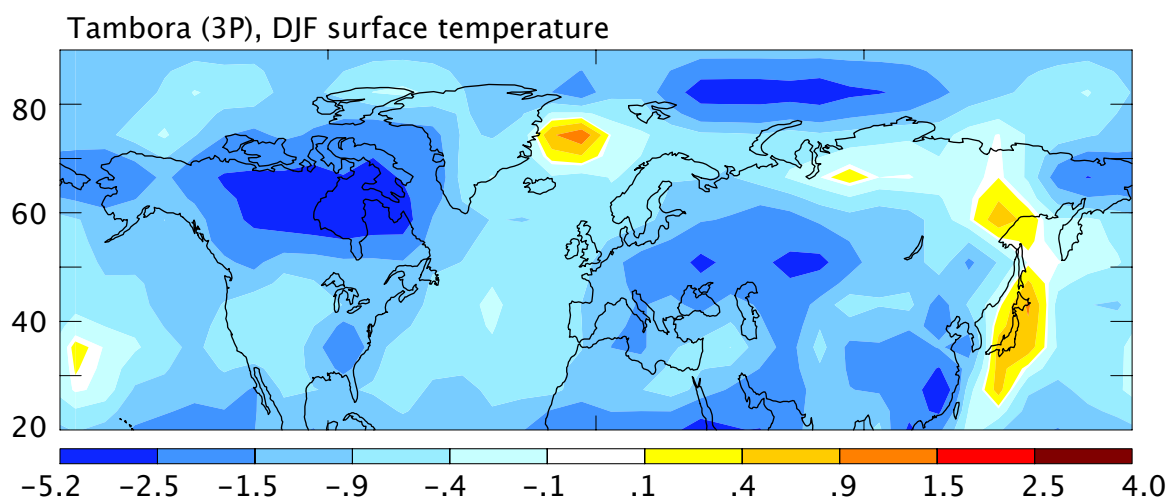Zonal-Mean Optical Thickness at 550 nm

| 0 | .002 | .003 | .006 | .01 | .02 | .03 | .06 | .1 | .2 | .3 |

Figure 2

Pinatubo, DJF surface temperature

Pinatubo, NDJFMA sea level pressure

Figure 3

Tambora (3P), DJF surface temperature

−5.2 −2.5 −1.5 −.9 −.4 −.1 .1 .4 .9 1.5 2.5 4.0

Tambora (3P), NDJFMA sea level pressure

−3.8 −1.6 −1.2 −.9 −.5 −.2 .2 .5 .9 1.2 1.6 3.2

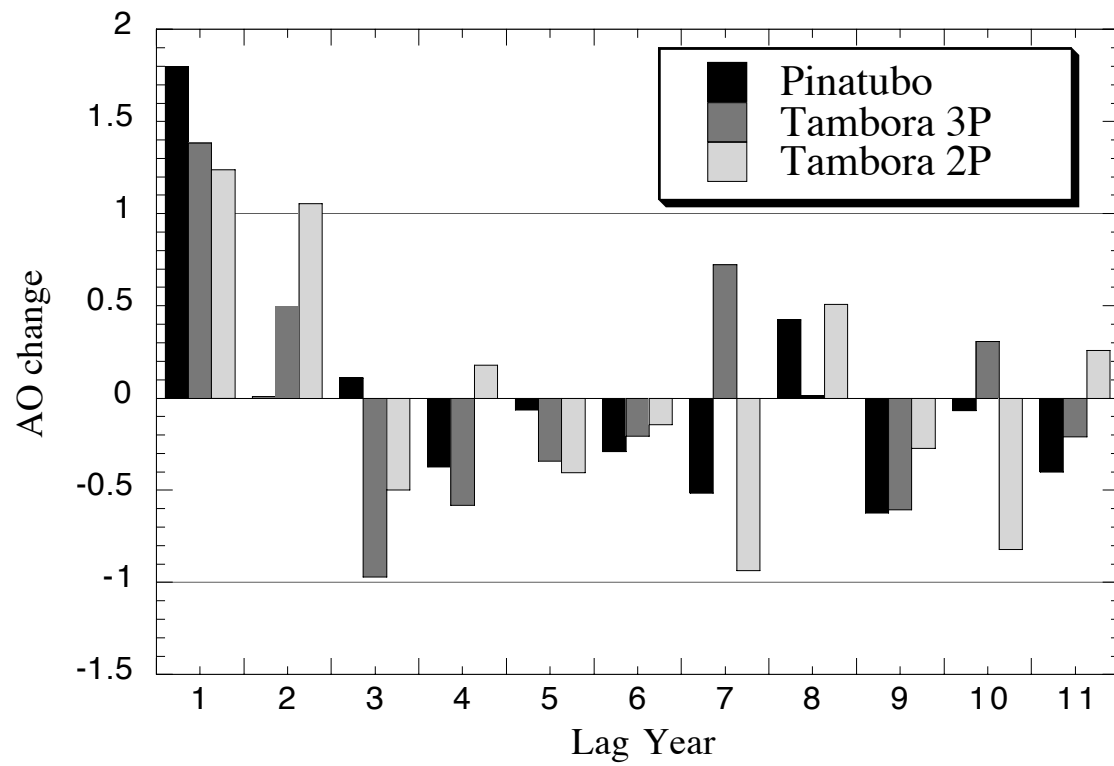Tambora (2P), DJF surface temperature
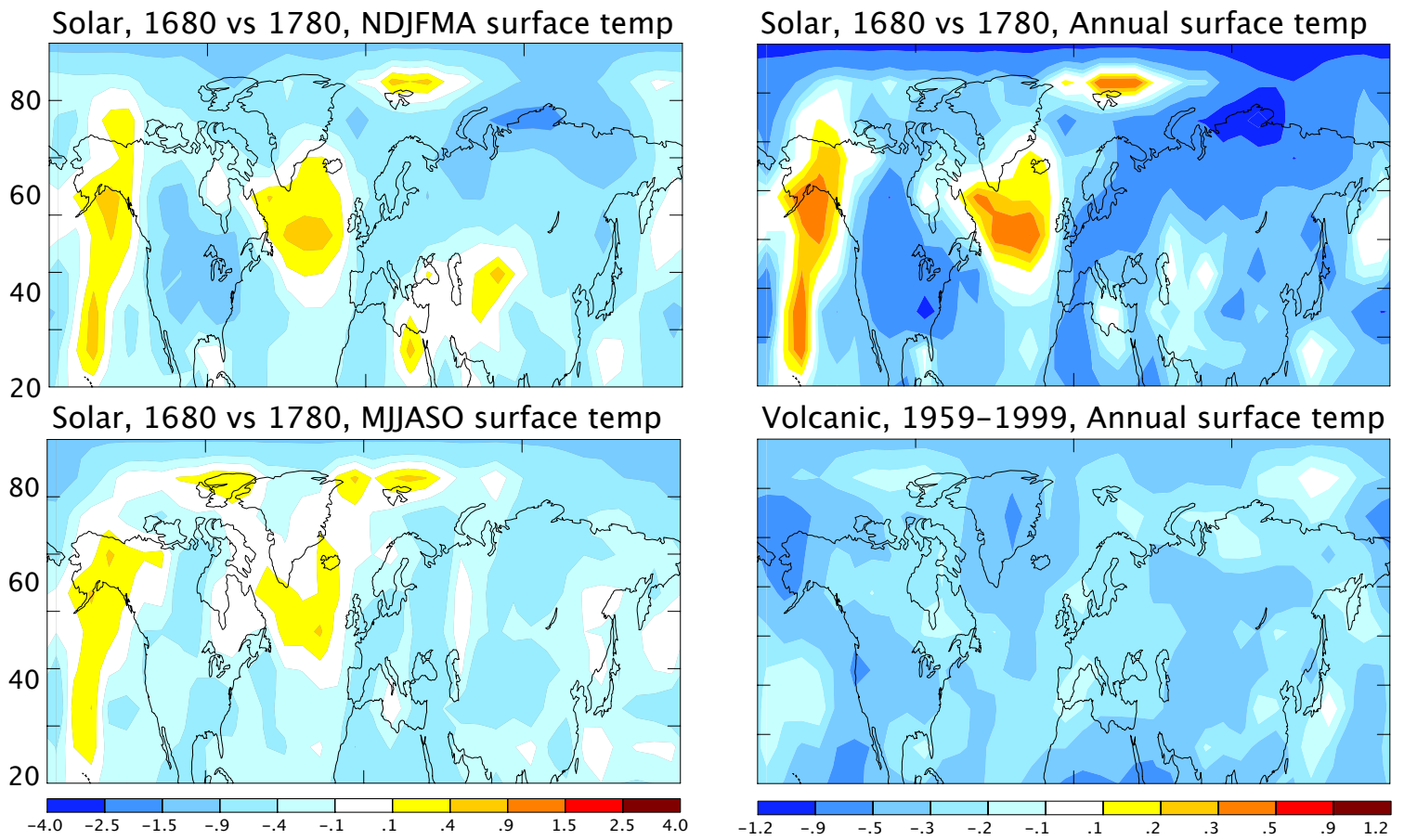
−4.4 −2.5 −1.5 −.9 −.4 −.1 .1 .4 .9 1.5 2.5 4.1
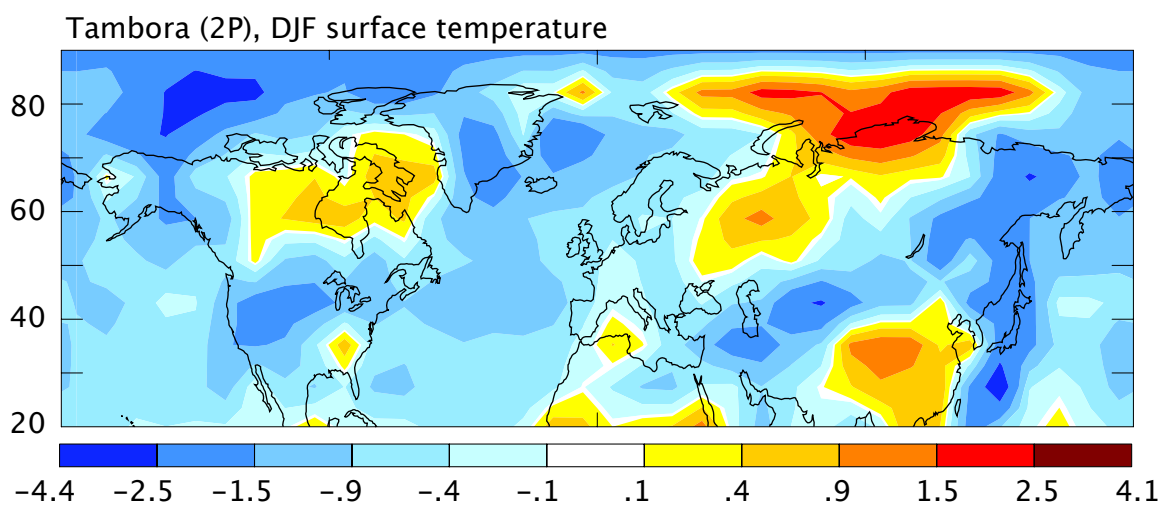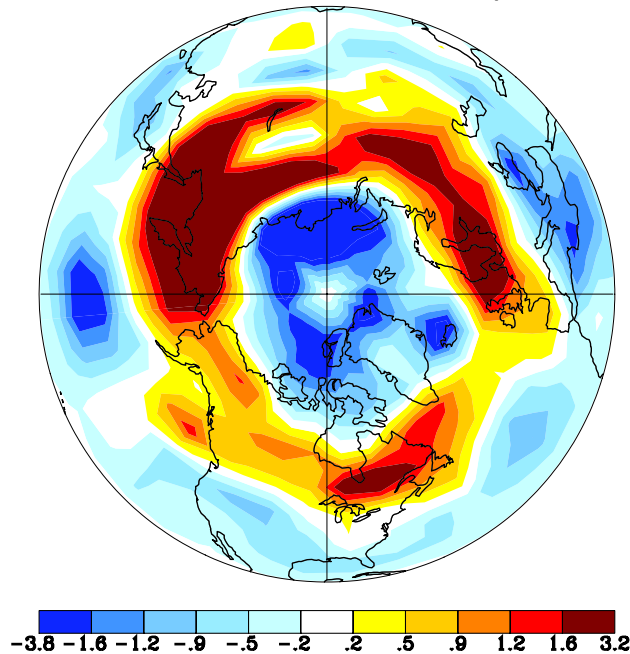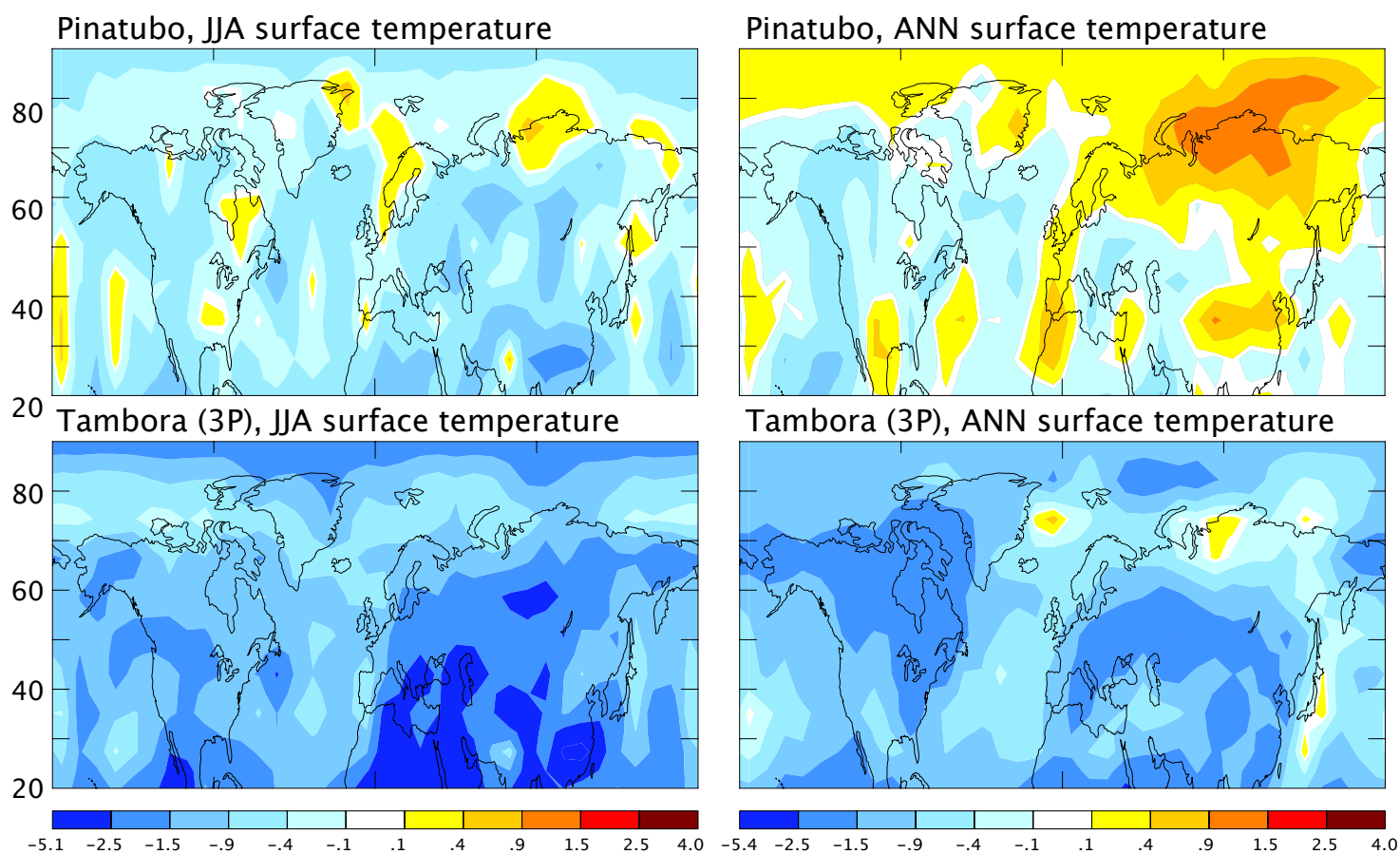
Figure 4

Figure 5

Figure 6

Figure 7

Figure 8

Proxy data reconstruction, 1660–80 vs 1770–90, ANN surface temperature

GCM simulation, 1680 vs 1780 solar + volcano, ANN surface temperature